Boron Doped Nanocrystalline Diamond Films for Biosensing Applications

V. Petrák, J. Krucký, M. Vlčková

Abstract

With the rise of antibiotic resistance of pathogenic bacteria there is an increased demand for monitoring the functionality of bacteria membranes, the disruption of which can be induced by peptide-lipid interactions. In this work we attempt to construct and disrupt supported lipid membranes (SLB) on boron doped nanocrystalline diamond (B-NCD). Electrochemical Impedance Spectroscopy (EIS) was used to study in situ changes related to lipid membrane formation and disruption by peptide-induced interactions. The observed impedance changes were minimal for oxidized B-NCD samples, but were still detectable in the low frequency part of the spectra. The sensitivity for the detection of membrane formation and disruption was significantly higher for hydrogenated B-NCD surfaces. Data modeling indicates large changes in the electrical charge when an electrical double layer is formed at the B-NCD/SLB interface, governed by ion absorption. By contrast, for oxidized B-NCD surfaces, these changes are negligible indicating little or no change in the surface band bending profile.

Keywords: biosensor, nanocrystalline diamond, electrochemical impedance spectroscopy.

1 Introduction

The increase in antibiotic resistance of pathogenic bacteria strains has spurred the development of novel antibiotics. One promising solution to these problems is the group of antibiotics based on antimicrobial peptides which are an abundant and diverse group of molecules that are produced by many tissues and cell types in a variety of plant and animal species. Their amino acid composition, amphipathicity, cationic charge and size allow them to attach to membrane bilayers and disrupt the membrane by the formation of pores [1]. They do not target specific molecular receptors on the microbial surface, but rather interact directly with microbial membranes, which they can rapidly permeabilize. The monitoring of specific peptide-lipid interactions in antibiotic peptides, which affect the functionality of bacterial membranes, can play an important role in the research of new antibiotics [2].

Supported lipid bilayers (SLBs) are investigated as model systems of biological membranes. They are composed of a lipid bilayer adsorbed on the surface of a solid substrate. In past decades, lipid membranes on a solid substrate have attracted considerable interest, from the point of view of both fundamental and applied science. These structures have been extensively used to study the structure and properties of native biological membranes and for investigating biological processes such as molecular recognition, enzymatic catalysis, membrane fusion and cell adhesion [3]. In addition, several applications based on lipid membranes have been developed, including the design of biosensors.

A well-established technique for the formation of SLBs is the Langmuir–Blodgett technique, which is carried out by pulling a hydrophilic substrate through a lipid monolayer and sequentially pushing it horizontally through another lipid monolayer [4]. A second commonly employed technique for forming SLBs is vesicle fusion, in which a supported bilayer is formed by the adsorption and fusion of vesicles from an aqueous suspension to the solid substrate surface [5].

Commonly used substrates for SLBs are mica, fused silica and glass. Other substrates such as silicon, SiO_2, platinum and gold have also been reported. In the case of diamond, SLBs can be formed on an oxidized hydrophilic surface and also on a hydrogenated hydrophobic surface [6]. Diamond exhibits several special properties, such as good biocompatibility and a large electrochemical potential window. These properties make diamond particularly suitable for biosensing [7].

In this application, a boron doped nanocrystalline diamond (B-NCD) film serves as a solid support for SLBs and an active electrode for electrochemical impedance spectroscopy (EIS) measurement of melittin induced membrane disruption. EIS was successfully used for detection of disruption by melittin on a free-standing lipid bilayer as well as on SLBs on gold surfaces. Ang et al. were able to detect membrane disruption of SLBs caused by Maigainin II on optically transparent diamond [6]. The EIS detection of

membrane disruption by antimicrobial peptide LL-37 has also been demonstrated. This work focuses on the effects of surface termination on the detection abilities of B-NCD film.

In the present work we have constructed a simple sensor for detecting the disruption of SLBs formed on a semi-metallically boron doped NCD electrode that serves as a working electrode. SLBs are disrupted by membrane active peptide melittin. We report the results of EIS of membrane disruption on hydrogenated and oxidized surfaces, and discuss the influence of B-NCD surface termination on the sensitivity of the sensor.

2 Experimental

Planar sensor electrodes were prepared by microwave plasma-enhanced chemical vapor deposition (MW PE-CVD) from methane/hydrogen mixtures in an ASTeX reactor, as described in [8]. The substrates were 2 inch silicon wafers (thickness 550 μm, crystalline orientation (100), p-type doped with boron and resistivity from 1 to 20 Ω·cm), which were diced into samples 10 mm by 10 mm after deposition. The diamond layers had a typical thickness of 150 nm with an average grain size of 50 nm, as determined by X-ray diffraction and atomic force microscopy. To ensure good electrical conductivity of the diamond layer, the CVD deposition was performed with an admixture of trimethylboron to the CH_4 gas with a concentration ratio of 200 ppm B/C. The B NCD samples served as the working electrode in our home-made set-up that allows impedance read-out.

Prior to the measurements, the diamond samples were either hydrogenated in H_2 plasma (50 Torr, 800 °C, power 4 000 W, duration 15 min) or oxidized by UV-ozone for 30 minutes. For the evaluation, the resulting contact wetting-angles were $95° \pm 2°$ for the hydrogenated diamond and $14° \pm 3°$ for the oxidized diamond. The B-NCD samples were cleaned in a mixture of H_2SO_4/KNO_3 (2 : 1 wt%) heated to 250 °C for 10 minutes. The samples were then rinsed in deionized water and dried under a stream of nitrogen.

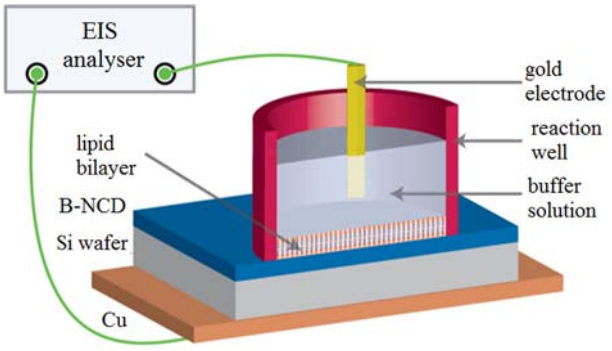

Fig. 1: A schematic cross-section of the setup for EIS measurements

The B-NCD samples were mounted on a copper backing contact, using an electrically conductive eutectic transfer tape. Rubber O-rings (Viton) with an inner diameter of 6 mm were pressed between the active electrode and the body of the sensor, forming a cell with a total inner volume of 160 μl. The cell was filled with 140 μl of 10 mM Hepes buffer solution. A gold counter electrode 500 μm in diameter was immersed in the solution. The working and counter electrode were connected to the 4194A Impedance/Gain-Phase Analyser (Hewlett Packard, USA) with shielded cables.

After a stable signal was obtained at 25 °C, a 100 μM solution of DOPC : DOPS (1 : 4) liposomes with negative charge was added. The membrane was formed by the vesicle fusion method. Lipid membrane formation was completed within 30 minutes. For membrane disruption, a 2 μM active amphipathic α-helical peptide, melittin, was added.

The impedance measurement, 10 mV AC potential signal (U) was applied and the resulting AC current was measured (I). Each 15 seconds, a sweep of 50 frequencies ranging from 100 Hz to 1 MHz was done.

2.1 Equivalent circuit

The equivalent circuit used for modeling the EIS data was used for diamond to model the processes in the sensor in several other applications [9]. The equivalent circuit, shown in Figure 2, can be divided into three components. (1) The first component is the series resistance R_S. This comprises the solution and the electrode resistance between the gold and the B-NCD working electrode. (2) The second component is a parallel combination of resistance R_1 and a constant phase element Q_1, and corresponds to the double layer on the surface of the electrode. (3) The third component, which corresponds to the space-charge region in the B-NCD, also consists of a parallel combination of resistance R_2 and a constant phase element Q_2. The data was fitted to the model in ZSimpWin (Princeton Applied Research, USA). The quality of the fit is determined by the χ^2 test. If the result is below $1 \cdot 10^{-3}$ it is a good assumption that the model that was used is correct.

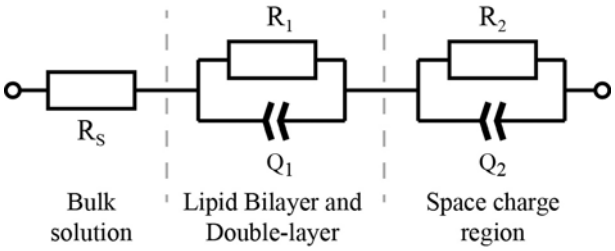

Fig. 2: The equivalent circuit used for modeling divided into components. R represents resistance; Q is a constant phase element

3 Results

The data series were fitted over the total measured frequency range from 100 Hz to 1 MHz. The resistance of the solution was calculated from 8 measurements, and was found to be 99 Ω ± 12 Ω. The constant phase elements in the equivalent circuit showed a value of n close to 1, suggesting the capacitance character of the circuit element.

3.1 SLB on oxidized B-NCD

The lipid membrane was measured directly during its formation and subsequently the melittin induced disruption was measured by EIS. The modeling showed significant changes in the equivalent circuit related to the formation of the lipid membrane. The Nyquist plot in Figure 3 consists of a semicircle in the higher frequency part of the spectra, which represents the space charge region, and the second semicircle in the lower frequency corresponds to the interface capacitance.

The change in the absolute value of the impedance upon formation of the membrane on the surface was low. However, the change was detectable at low frequencies, as can be seen on the Nyquist plot in Figure 3. The absolute impedance value at a frequency of 255 Hz had risen from 1 453 to 1 540 Ω.

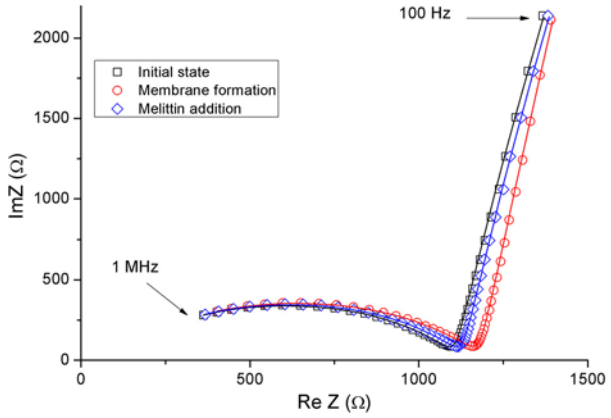

Fig. 3: Nyquist plot showing the initial state prior to addition of liposomes (□), state after membrane formation (▽) and addition of melittin (◇). Fits to the equivalent circuit are indicated with solid lines

After membrane formation, the free liposomes in the solution were flushed with 1 mM Hepes buffer. The changes in impedance were minimal in the entire frequency range and remained at a value of 1 540 Ω for a frequency of 255 Hz. The same is true for the equivalent circuit values, which remained almost unchanged.

After the addition of melittin, the difference in the high frequency part was minimal. However, a small change was observed in the impedance spectra. The absolute value of the impedance at a frequency of 255 Hz decreased from 1 540 to 1 461 Ω. The maximum change of the absolute impedance value during the measurement was only 5 % during the disruption.

3.2 SLB on an hydrogenated B-NCD

The first curve (□) in Figure 4 shows the initial state, when only Hepes buffer was present, and the second curve (○) shows the result state after the addition of liposomes. An increase in the size of the semicircle corresponding to the molecular bilayer on the B-NCD surface can be seen on the Nyquist plot. The modeling showed that the main detectable change in the equivalent circuit was a decrease in resistance R_1 from 55 to 28 kΩ, together with a change in the capacitance of the constant phase element Q_1 from 279 nF to 141 nF. By contrast, the resistance value represented by the R_2 capacitance of Q_2 changed from 0.45 nF to 1.38 nF. The absolute value of the impedance at a frequency of 4.9 kHz rose from 4.4 to 7.6 kΩ, so the impedance rose by 175 % of the value prior to addition.

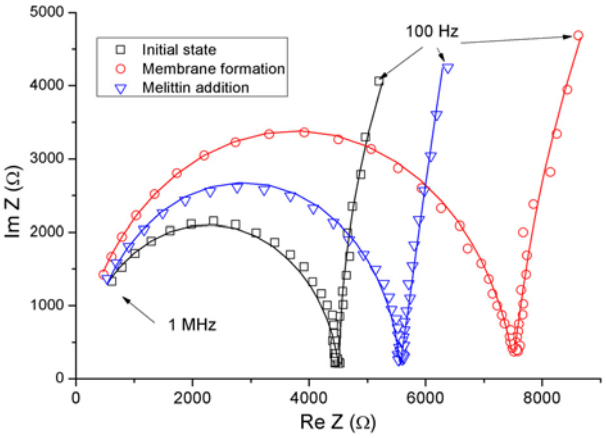

Fig. 4: Nyquist plot representing changes in impedance after the addition of liposomes (□), state after membrane formation (○) and the addition of melittin (▽). Fits to the equivalent circuit are indicated with solid lines. The change after the addition of liposomes into the solution and after membrane disruption is clearly visible

Redundant free liposomes in the solution were subsequently flushed with 1 mM Hepes buffer. The flush of the liposomes did not result in any significant change in the impedance characteristic, and the absolute value of the impedance changed only from 7.6 to 7.5 kΩ. This represents a 2 % change in the impedance at 4.9 kHz frequency.

The membrane active peptide, melittin, was added after the system had stabilized. The absolute value of the impedance at a frequency 5 KHz decreased from 7.5 to 5.2 kΩ. This represents 68 % of

the impedance value before the addition of melittin. Data modeling using the equivalent circuit showed a change in the values of the $R_1 \parallel Q_1$ elements of the circuit. The values of elements R_1, Q_1 increased. The resistance of R_1 increased from 28 to 41 kΩ and the capacitance of Q_1 increased from 141 nF to 356 nF. However, the resistance of R_2 decreased from 7.3 to 5.1 kΩ, and the capacitance of Q_2 changed from 1.35 nF to 0.83 nF.

3.3 Comparison of hydrogenated and oxidized surfaces

The main difference in sensitivity can be attributed to the difference in hydrogenated and oxidized surfaces. In the case of a hydrogenated surface, the band bending is upwards, and the addition of negative charge SLB at the surface leads to increased band bending. By contrast, in the case of an oxidized surface the band bending is downwards, and the addition of SLB should reduce the surface band bending. However, the important fact is that we are working with B-NCD, in which free holes are present. When we add the negatively charged SLB on a hydrogenated surface and increase the negative charges at the surface, the holes from B-NCD diffuse to the B-NCD surface, leading to a large change in the impedance of the system. On the other hand, when we work with an oxidized surface there are no free electrons in B-NCD and therefore the change in the surface band bending is limited. This is the main reason why the B-NCD sensor will work much more effectively with hydrogenated surfaces.

4 Conclusions

An impedimetric characterization of membrane formation and disruption on a hydrogenated and oxidized B-NCD surface has been carried out. For a hydrogenated surface, significant changes have been observed in the properties of the B-NCD/SLB interface on interacting with the membrane active peptides. Data modeling indicated large changes in the electrical charge occurring at the diamond surface, and also the creation of an electric double layer at the B-NCD/SLB interface, which is governed by ion-absorption. By contrast, for an oxidized B-NCD surface, these changes are negligible. This indicates that there are few or no changes to the surface band bending profile.

Acknowledgement

The research described in this paper was supervised by Prof. Patrick Wagner from Hasselt University and Prof. Milos Nesladek from the Faculty of Biomedical Engineering, Czech Technical University in Prague.

Financial support from the Academy of Sciences of the Czech Republic (grants KAN200100801 & KAN400480701), COST MP0901 — NanoTP, MSM6840770012 "Transdisciplinary Research in the Field of Biomedical Engineering II". and CTU (grant No. CTU 10/811700) are gratefully acknowledged. The Erasmus student exchange programme is also gratefully acknowledged.

References

[1] Izadpanah, A., Gallo, R. L.: Antimicrobial Peptides, *Journal of the American Academy of Dermatology*, vol. **52**, no. 3, 52, p. 381–390.

[2] Castellana, E. T., Cremer, P. S.: Surface Science Reports, *Solid supported lipid bilayers*, vol. **61**, no. 10, p. 429–444.

[3] Dufrene, Y. F., Lee, G. U.: Advances in the characterization of supported lipid films with the atomic force microscope, *Biochimica et Biophysica Acta – Biomembranes*, vol. **1 509**, no. 1–2, p. 14–41.

[4] Solletti, J. M., Botreau, M., Sommer, F., Brunat, W. L., Kasas, S., Duc, T. M., Celio, M. R.: Elaboration and Characterization of Phospholipid Langmuir-Blodgett Films, *Langmuir*, vol. **12**, no. 22, p. 5 379–5 386.

[5] Kalb, E., Frey, S., Tamm, L. K.: Formation of supported planar bilayers by fusion of vesicles to supported phospholipid monolayers, *Biochimica et Biophysica Acta*, vol. **1 130**, no. 2, p. 307–316.

[6] Ang, P. K., Loh, K. P., Wohland, T., Nesladek, M., Van Hove, E.: Supported Lipid Bilayer on Nanocrystalline Diamond Dual Optical and Field-Effect Sensor for Membrane Disruption, *Advanced Functional Materials*, vol. **19**, p. 109–116.

[7] Nebel, C. E., Rezek, B., Shin, D., Uetsua, H., Yang, N.: Diamond and biology, *Journal of the Royal Society Interface*, vol. **4**, p. 439–446.

[8] Williams, O., Nesladek, M. et al.: Growth, electronic properties and applications of nanodiamond, *Diamond and Related Materials*, vol. **17**, no. 7–10, p. 1 080–1 088.

[9] Vermeeren, V., Daenen, M., Grieten, L., et al.: Diamond-based DNA sensors: surface functionalization and read-out strategies, *Physica Status Solidi A*, vol. **260**, no. 3, 520(2009).

About the authors

Václav Petrák was born in Prague, Czech Republic. He graduated with a master degree from the Faculty of Biomedical Engineering of the Czech Technical University in Prague in 2010. In 2008 he joined department of Functional Materials at the Institute of Physics of the Academy of Sciences of the Czech Republic. In 2010 he worked for 5 months at the Institute of Material Research in Hasselt (Belgium) during his Erasmus student exchange. He is currently working on his doctoral thesis. His professional interests are nanocrystalline diamond, nanodiamond particles, biosensors, and also neural circuits and data analysis. His personal interests are family, traveling and photography.

Jaroslav Krucký was born in Prague, Czech Republic. He graduated with a bachelor degree from the Faculty of Biomedical Engineering of the Czech Technical University in Prague in 2009. In 2009 he joined the department of the Functional Materials at the Institute of Physics of Academy of Sciences. He is currently working on methods for preparing ND thin films with selective growth. In future, he is planning to work on diamond micro-electron array electrodes for in vivo and in vitro neural measurements.

Marie Vlčková graduated with a bachelor degree from the Faculty of Biomedical Engineering of the Czech Technical University in Prague in 2010. She is continuing her studies at FBMI, and is currently working on optimization of the surface pretreatment of substrates for diamond CVD deposition. Her professional interests are biomedical applications of diamond films.

Václav Petrák
E-mail: vaclav.petrak@fbmi.cvut.cz
Jaroslav Krucký Marie Vlčková
Department of Biomedical Technology
Faculty of Biomedical Engineering
Czech technical University, Kladno, Czech Republic